catalysts

MDPI

Article

ZnO-Bi_2O_3 Heterostructured Composite for the Photocatalytic Degradation of Orange 16 Reactive Dye: Synergistic Effect of UV Irradiation and Hydrogen Peroxide

Roeel Shahzad [1,2], Majid Muneer [1,*], Rimsha Khalid [2] and Hatem M. A. Amin [3,4,*]

[1] Department of Chemistry, Government College University Faisalabad, Faisalabad 38000, Pakistan; rueelshehzad@gmail.com
[2] Institute of Chemistry, University of Sargodha, Ibne Sina Block, Sargodha 40100, Pakistan; rimshakhalid239@gmail.com
[3] Chemistry Department, Faculty of Science, Cairo University, Giza 12613, Egypt
[4] Analytical Chemistry II, Faculty of Chemistry and Biochemistry, Ruhr University Bochum, 44801 Bochum, Germany
* Correspondence: majidmuneer@gcuf.edu.pk (M.M.); hatem@pc.uni-bonn.de (H.M.A.A.)

Abstract: The development of semiconductor photocatalysts has recently witnessed notable momentum in the photocatalytic degradation of organic pollutants. ZnO is one of the most widely used photocatalysts; however, its activity is limited by the inefficient absorption of visible light and the fast electron–hole recombination. The incorporation of another metal or semiconductor with ZnO boosts its performance. In this present study, a heterostructured ZnO-Bi_2O_3 composite was synthesized via a simple co-precipitation method and was investigated for the UV-driven photocatalytic degradation of the Reactive Orange 16 (RO16), a model textile dye. The successful fabrication of ZnO-Bi_2O_3 microstructures with crystalline nature was characterized using X-ray diffraction (XRD), Fourier transform infrared spectroscopy (FTIR), scanning electron microscopy (SEM), and energy-dispersive X-ray (EDX). The discoloration of the dye solution was quantified using UV–Vis spectroscopy to determine the photocatalytic efficiency. The photocatalytic activity results demonstrated that the photodegradation at ZnO-Bi_2O_3 heterojunction was more efficient and 300 and 33% faster than individual Bi_2O_3 and ZnO catalysts, respectively, an effect that is indicative of a synergistic effect. In the presence of ZnO-Bi_2O_3 particles, the UV light-driven activity for RO16 degradation was twice as high as in its absence. The influence of adding the oxidant H_2O_2 on the UV-induced photocatalytic degradation was investigated and the results revealed a two-time increase in the photocatalytic activity of ZnO-Bi_2O_3 compared to UV irradiation alone, which could be ascribed to a summative degradative effect between UV and H_2O_2. Hence, this approach holds the potential for environmentally friendly wastewater treatment.

Keywords: orange 16 dye; photocatalysis; ZnO; Bi_2O_3; hydrogen peroxide; degradation kinetics

Citation: Shahzad, R.; Muneer, M.; Khalid, R.; Amin, H.M.A. ZnO-Bi_2O_3 Heterostructured Composite for the Photocatalytic Degradation of Orange 16 Reactive Dye: Synergistic Effect of UV Irradiation and Hydrogen Peroxide. *Catalysts* **2023**, *13*, 1328. https://doi.org/10.3390/catal13101328

Academic Editor: Edward G. Gillan

Received: 10 August 2023
Revised: 19 September 2023
Accepted: 22 September 2023
Published: 28 September 2023

1. Introduction

The textile industry is known for its extensive use of dyes in the manufacturing process and thus releases a large amount of wastewater containing toxic chemicals into water bodies [1]. These textile dyes are often non-biodegradable and can cause threats to aquatic ecosystems and human health [2]. For instance, the inhalation of dye particles can cause severe respiratory problems. In addition, when untreated dye effluents and other carcinogenic substances are discharged into water resources, they can contaminate drinking water sources, jeopardizing the health and well-being of communities that depend on them [3,4]. The metal complex-containing dyes can release toxic heavy metals into watercourses, posing a detrimental risk to the environment and humans. Among other textile dyes, reactive dyes are highly soluble in water, rendering their removal through conventional methods difficult [5].

It is essential to develop efficient treatment strategies. A range of conventional treatments has been investigated for the decolorization of textile effluents, including chemical oxidation [6], biodegradation, adsorption, and electrochemical degradation. These approaches have their advantages and disadvantages. For instance, although the physico-chemical methods are successful, they encounter issues with the generated sludge disposal, the formation of toxic byproducts, the high cost of operation, chemicals, and electricity [7,8]. A drawback of biodegradation is the need for a suitable environment for the microorganisms to thrive as well as the difficulty of upscaling [9]. In contrast, photodegradation provides a sustainable efficient alternative to degrading dyes under light irradiation into colorless, less hazardous waste that can be released without compromising their physicochemical properties [1,10].

Semiconductor photocatalysts are used for this photocatalytic degradation process. Among others, TiO_2 and ZnO are widely used as photocatalysts [11–14]. The advantages of photocatalysis for dye discoloration include high efficiency, no need for hazardous chemicals, being environmentally benign, being relatively cost-effective, and versatility [10,15]. However, photocatalysis has some limitations, such as the need for a light source and the possible deactivation of the photocatalyst over time. Furthermore, variables like the type of dye that is degraded, and the specific conditions of the treatment process can affect how effective photocatalysis is. Additionally, the effectiveness of photocatalysis can vary depending on factors such as the chemical composition and structure of the dye being degraded. To address these limitations, it is essential to carefully assess the specific situation and goals when choosing a method for dye degradation.

ZnO is recognized as an outstanding semiconductor in photocatalysis [16]. ZnO is an n-type semiconductor [17] with a large band gap of about 3.2 eV [15]. It is a non-toxic, cost-effective, and thermally and chemically stable material with simplicity of manufacture. For example, ZnO nanoparticles (NPs) were synthesized using an extract of *Punica granatum* plant and were able to degrade textile orange 16 reactive dye with an overall efficiency of 93% [16]. However, the photo-efficiency of ZnO is often limited by the inefficient absorption of visible light as well as the fast electron–hole recombination [15,18]. A promising strategy to improve ZnO photocatalytic performance is the formation of a heterojunction with other metallic or oxide semiconductors such as Bi_2O_3. This approach has proven to be effective in extending the spectral response of the hybrid system and favors charge separation, thus boosting the photocatalytic activity and stability [19,20].

Generally, improving the photocatalytic activity via synergistically combining two different metals or semiconductors has been reported as an efficient strategy [21]. For instance, Wang et al. [22] demonstrated the high efficiency of Ni-Pd/Fe_3O_4 yolk-shelled nanospheres for the catalytic reduction of N-containing dyes. These magnetic nanocomposites, with uniformly dispersed Ni and Pd, exhibit excellent recyclability and enhanced catalytic activity for various dyes compared to single metal counterparts (Ni/Fe_3O_4 and Pd/Fe_3O_4). The Au@CoP metal–semiconductor hybrid also showed improved photocatalysis performances for rhodamine 6G dye [23]. Such summative positive effect was also observed for the hybrid photocatalyst containing ZnO and β-cyclodextrin (β-CD) particles, and this composite exhibited 100% removal efficiency for ceftriaxone [24]. In this regard, integrating two oxide semiconductors to obtain optimum energy levels in the heterojunction that match the redox potentials of the involved radical generation reactions would be beneficial.

In this context, Bi_2O_3 is a p-type semiconductor [17] with a bandgap in the range of 2.1 to 3.1 eV [25,26]. Bi_2O_3 can possibly generate active radicals such as superoxide (O_2^-) from water that could initiate dye oxidation processes. A few studies reported the synthesis of heterostructures of ZnO-Bi_2O_3 for improved photocatalytic activity against dyes. For example, ZnO with 6.8–18.9 wt% α- Bi_2O_3 nanostructures was reported, and this heterostructure demonstrated a higher discoloration rate of acid black under UV irradiation as compared to the respective single oxides [19]. Wang et al. [27] showed that a 5% molar ratio of the ZnO/α-Bi_2O_3 nanomaterial, prepared by a solid-state reaction, has the best photo-discoloration ability under sunlight for Rhodamine B, which was attributed to the

effective separation of charge carriers. OH radicals were revealed as the main active species for the discoloration of this dye over this ZnO/α- Bi_2O_3. A synergistic effect in ZnO/Bi_2O_3 heterostructure was reported as a reason for the improved photodegradation performance for indigo carmine dye compared to individual ZnO and Bi_2O_3 [20]. During the photo-oxidation process, powerful oxidative radicals such as $^{\bullet}OH$, H_2O_2, and $O_2^{-\bullet}$ are produced from oxygen reduction and water splitting [28] and can oxidize dye molecules into lower molecular weight molecules (e.g., tiny inorganic compounds or minor aldehydes), CO_2, and water [29]. Moreover, in the presence of H_2O_2, UV radiation can be very effective in oxidizing dyes as UV (200–280 nm) causes H_2O_2 breakdown, generating $^{\bullet}OH$ radicals that can efficiently degrade reactive dyes [30].

Motivated by some of the leading studies mentioned above, this work reports on the facile synthesis of a ZnO-Bi_2O_3 hybrid composite via a co-precipitation method. The synthesized material was characterized using the SEM, EDX, XRD, and FTIR methods. The photocatalytic performance of the prepared ZnO-Bi_2O_3 catalyst was evaluated for the Reactive Orange 16 (RO16) dye, as a model dye, under UV irradiation. Furthermore, the influence of the addition of H_2O_2 as a radical source on the dye degradation rate was assessed and the results manifested an improved degradation efficiency when UV irradiation was combined with H_2O_2 compared to only UV exposure. The kinetics of degradation was also determined. Based on the band gap energy and redox potentials of possibly involved reactions, a proposed mechanism of photocatalysis and degradation via the ZnO-Bi_2O_3 hybrid was discussed.

2. Results and Discussion

2.1. Structural and Morphological Characterization of the ZnO-Bi_2O_3 Heterojunction

2.1.1. Crystalline Structure Using XRD Analysis

The as-synthesized ZnO-Bi_2O_3 particles were systematically characterized using various techniques. The crystalline structure of the synthesized particles was determined using powder X-ray diffraction (XRD). Figure 1 compares the experimental XRD pattern of ZnO-Bi_2O_3 with the standard patterns of ZnO and Bi_2O_3. The XRD pattern of ZnO-Bi_2O_3 exhibited distinct Bragg reflections that were assigned to the crystal planes of both ZnO and Bi_2O_3. Specifically, the ZnO peaks were observed at 2θ values of 31.9°, 35.2°, 38.2°, 47.3°, 56.8°, 63.1°, 66.6°, 68.1° and 69.3° corresponding to the (100), (002), (101), (102), (110), (103), (200), (112) and (201) crystal planes, respectively [29]. The pattern is closest to the hexagonal structural of ZnO with space group P63mc (186) according to the PDF card No. 36–1451 [15]. The Bi_2O_3 peaks were observed at 2θ of 26.1°, 31.9°, 32.7°, 33.7°, 41.2°, 46.9°, 54.3°, 55.3°, 58.8°, and 66.6° corresponding to the (210), (002), (220), (102), (212), (400), (203), (421), (412), (004), and (421) crystal planes, respectively, which match the tetragonal structure of Bi_2O_3 with space group P-421c (114) (PDF card No. 27-0050) [31]. No diffraction peaks of impurities were present in the pattern. The above XRD reflections proved the presence of both ZnO and Bi_2O_3 in the prepared heterostructure ZnO-Bi_2O_3 in the study. In addition, the XRD peaks are sharp, suggesting the highly nanocrystalline nature of the ZnO-Bi_2O_3 crystallites. In addition, the crystallite size was calculated using the Debye–Scherrer equation as follows [32]:

$$D = \frac{K\,\lambda}{\beta\,\cos\theta} \quad (1)$$

where D is the nanoparticle crystalline diameter, K represents the Scherrer constant and equals 0.9, λ is the X-ray wavelength (1.54 Å for copper K-α), and β denotes the full width at half maximum (FWHM). An average crystallite particle size of the ZnO-Bi_2O_3 particles of 29.6 ± 7.1 nm was obtained from the analysis of the main reflections.

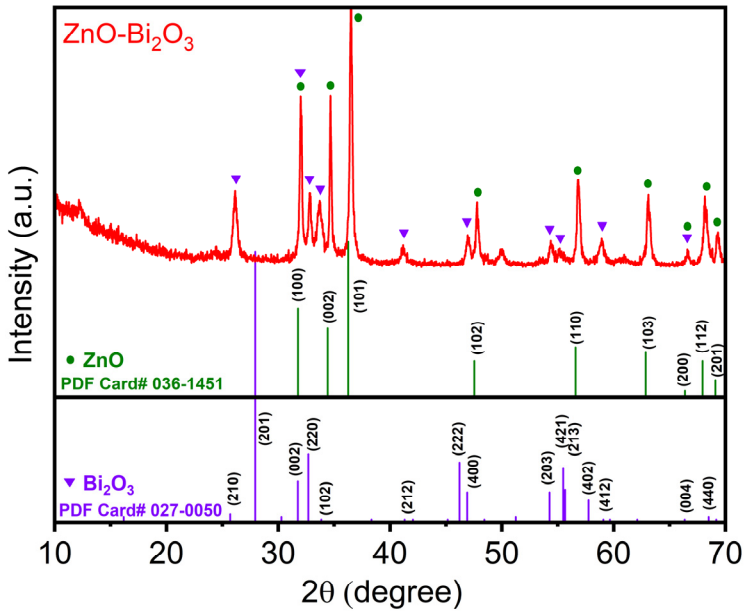

Figure 1. XRD patterns of the Zn-Bi_2O_3 sample as well as the standard PDF cards of ZnO and Bi_2O_3.

2.1.2. SEM Analysis

SEM analysis was conducted to investigate the morphological characteristics and surface topography of the ZnO-Bi_2O_3 heterostructured composite. SEM images of ZnO-Bi_2O_3 at two different magnifications are depicted in Figure 2a,b. SEM images revealed the formation microstructure with nanoparticles/aggregates of irregular shape. These images illustrate the formation of porous ZnO-Bi_2O_3 particles with a size in the range of 1–25 µm that comprise smaller particles grown on bigger ones. Further, the elemental analysis was performed using energy-dispersive X-ray (EDX) spectrometry, as presented in Figure 2c. The EDX spectrum results confirmed the presence of Zn, Bi, and O elements in the sample. The appearance of a smaller signal for Bi could be attributed to the expected small content of Bi (nominally 10 mol%) in the composite, and since EDX generally probes a few µm depth of the sample, a smaller amount of Bi in the probed volume would result in a relatively smaller signal. For our application, namely the degradation of dyes, the porous structure provides a high surface area, thus enhancing the contact between the composite material and the target dye. Hence, this increased surface area would facilitate the adsorption and photocatalytic degradation of RO16 dye. The porous nature of the particles further promotes mass transfer and diffusion of the target dye, facilitating enhanced photocatalytic degradation. Thus, the composite's unique properties, combining the photocatalytic activity of ZnO with the high surface area and catalytic capabilities of Bi_2O_3, are expected to improve degradation efficiency compared to individual components, thus creating a synergistic effect.

2.1.3. FTIR Spectroscopy

The FTIR analysis (Figure 3) of the ZnO-Bi_2O_3 photocatalyst reveals characteristic peaks that provide valuable insights into its chemical composition and functional groups. For example, the stretching vibration of Zn–O bonds was identified by a peak at 530 cm^{-1}, indicating the presence of ZnO in the composite [33]. Additionally, the peaks at 587 cm^{-1} and 840 cm^{-1} were assigned to the stretching vibrations of Bi–O–Bi bonds, confirming the incorporation of Bi_2O_3 into the composite structure [34]. These results are consistent with previous studies that have reported similar peak positions for Zn–O and Bi–O–Bi stretching vibrations in ZnO-Bi_2O_3 composites [33,34]. The peak at around 1405 cm^{-1} is often associated with the stretching vibration of the Zn–O bond. This peak represents the presence of ZnO in the composite and indicates the bonding between zinc and oxygen atoms [33]. On the other hand, the peak at 1500 cm^{-1} could be attributed to several possible vibrational modes in Bi_2O_3. For example, it might be related to the bending vibration

of the O–Bi–O bond or could arise from the stretching vibrations of the Bi–OH bond or the Bi–O–Bi bond [35]. The broad peak observed at 3400 cm^{-1} can be attributed to the stretching vibrations of OH bonds [36], indicating the presence of surface hydroxyl groups or adsorbed water molecules on the composite surface [37]. This finding infers the potential involvement of surface hydroxyl groups in the photocatalytic activity and the adsorption properties of the ZnO-Bi_2O_3 photocatalyst.

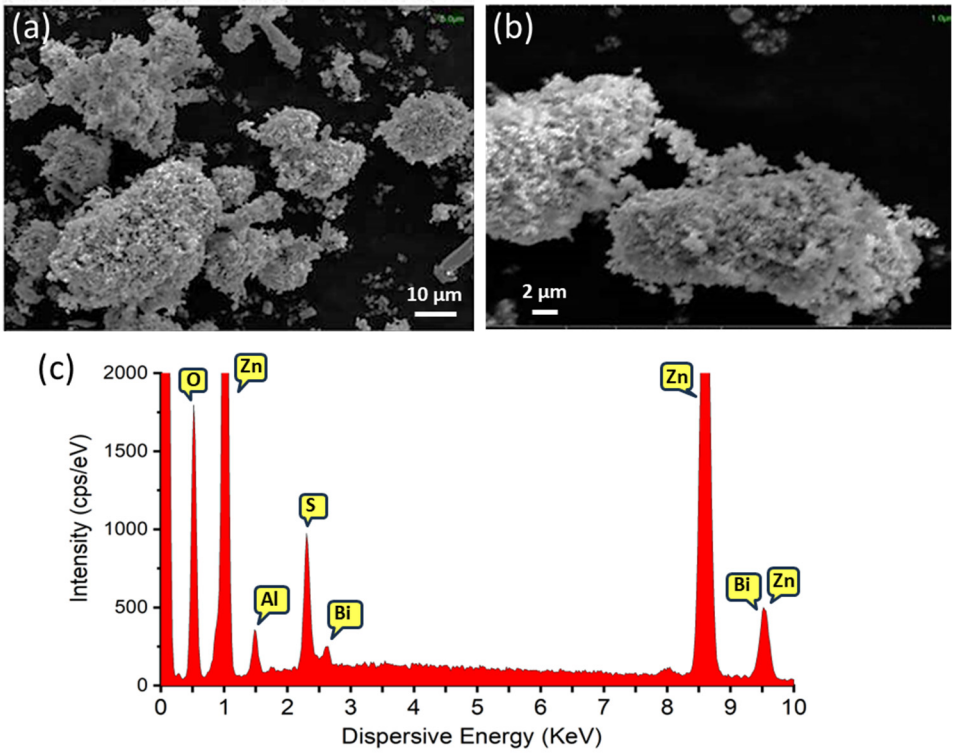

Figure 2. (**a**,**b**) SEM images of the composite ZnO-Bi_2O_3 particles at two different magnifications. (**c**) EDX spectrum of the composite.

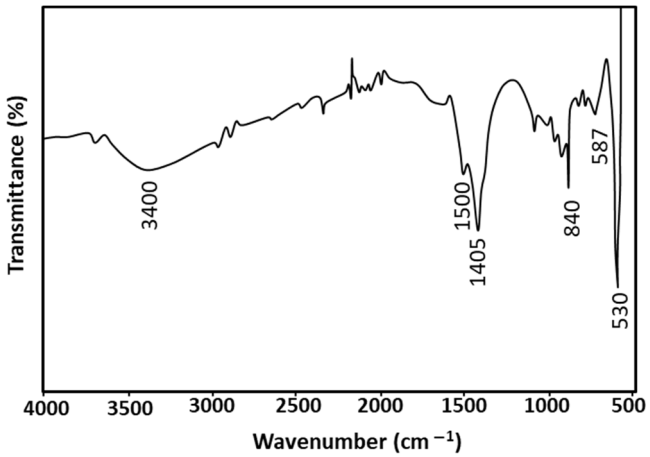

Figure 3. FTIR spectrum of the synthesized ZnO-Bi_2O_3 photocatalyst.

2.2. Evaluation of the Photocatalytic Activity of ZnO-Bi_2O_3

To evaluate the photocatalytic degradation and the band gap of the RO16 dye, the optical properties of this dye were initially investigated by recording the UV–Vis spectrum of a 100 ppm dye solution to identify the wavelength of maximum absorption (λ_{max}). Figure 4a shows the obtained spectrum, which exhibits a characteristic single strong

absorption peak at a wavelength of 488 nm. Accordingly, during the photolytic and photocatalytic studies, the change in absorbance was measured at the λ_{max} of 488 nm to assess the degradation of the dye under different experimental conditions. Since the band gap of the ZnO-Bi_2O_3 semiconductor is key to understanding the underlying photocatalytic mechanism in this catalyst, the band gap energy (E_g) was determined using Tauc's equation, as follows [38]:

$$(\alpha h\nu)^{1/n} = B\left(h\nu - E_g\right)^n \quad (2)$$

where α is the molar extinction coefficient, h the Plank's constant, ν represents the photon's frequency, B is a constant, and n depends on the type of the electron transition. The factor $n = 1/2$ and 2 for the direct and indirect band gaps, respectively [15]. The linearity of the plot and the absence of concave turning point between two linear segments in the plot of $(\alpha h\nu)^2$ versus $h\nu$ is characteristic of a direct band gap. The E_g was determined from the x-axis intercept of the tangent of the linear part of the plot of $(\alpha h\nu)^2$ versus $h\nu$, as shown in Figure 4b. The band gap energy for ZnO-Bi_2O_3 was found to be 3.13 eV, agreeing with literature values. This band gap of the heterojunction ZnO-Bi_2O_3 lies between the band gap energy of individual ZnO (3.3 eV) and Bi_2O_3 (1.8–2.7 eV), in agreement with previous reports [20,31]. These data indicate that the band gap of ZnO can be modified via the addition of Bi_2O_3.

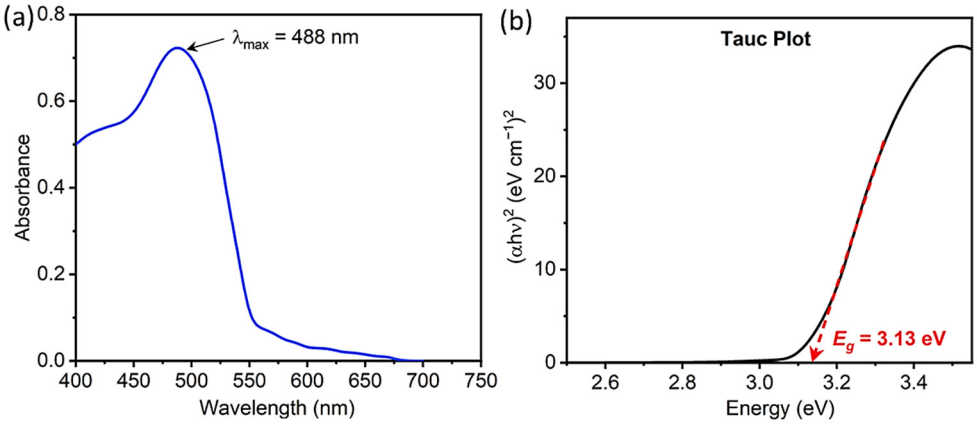

Figure 4. (**a**) UV spectrum of 100 ppm RO16 solution. (**b**) Respective Tauc plot to determine the band gap of the dye.

In this section, we evaluate the degradation of RO16 dye using the ZnO-Bi_2O_3 photocatalyst under UV radiation, both with and without the addition of hydrogen peroxide as an oxidizing agent. First, the photolysis experiments were evaluated and then the photocatalysis measurements in the presence of ZnO-Bi_2O_3 were assessed. To evaluate the degradation efficiency, the change in absorbance at 490 nm over time before and after each treatment was calculated. UV radiation has proven to be an effective method for the degradation of many dyes. Therefore, RO16 solutions were subjected to UV radiation alone or with the addition of H_2O_2 and in the presence of a catalyst combined with H_2O_2. The studied UV exposure durations ranged from 20 to 100 min. The results provided valuable insights into the effectiveness of the different treatment combinations and exposure times in degrading RO16 dye. These findings thus contribute to the understanding of UV-based degradation methods for the treatment of organic dye contaminants, specifically in the context of RO16 dye solutions.

2.2.1. Effect of Sole UV Irradiation on the Photolytic Degradation of RO16 Dye

In principle, the duration of UV irradiation directly influences the degradation extent of aqueous dye solutions. A longer exposure time to UV radiation leads to a higher percentage of dye degradation, indicating a direct relationship between exposure time and degradation efficiency [30]. In this context, it is desired to have a photocatalytic system with

a higher degradation rate. In the case of RO16, the initiation step of the degradation process involves the generation of hydroxyl radicals (•OH), which trigger the conversion of dye molecules to their excited state. This process results in the degradation of the chromophoric groups of the RO16 by breaking the N-N double bond. Consequently, the dye molecules repeatedly transition to the excited state, and the hydroxyl radicals continuously attack the dye molecules, leading to their degradation. Based on this proposed mechanism, it is expected that a longer exposure period to UV radiation promotes the degradation of the dye molecules [39]. The absorbance of various concentrations (100, 150, and 200 ppm) of RO16 dye solution at 490 nm was recorded before UV irradiation (0 min) and at different UV light exposure times (20, 40, 60, 80, and 100 min), as presented in Figure 5a. It was noticed that in the absence of UV irradiation, the absorbance of the dye solution did not decrease, indicating that the dye adsorption on the photocatalyst surface is negligible. As shown in Figure 5a, one can observe a monotonic decrease in the absorbance of the dye solution over time. Consequently, the degradation percentage increased with time but reached only 18% after 100 min for 200 ppm dye (Figure 5b). A similar trend in degradation percentage was obtained for all dye concentrations but with a higher absolute degradation % for higher concentrations.

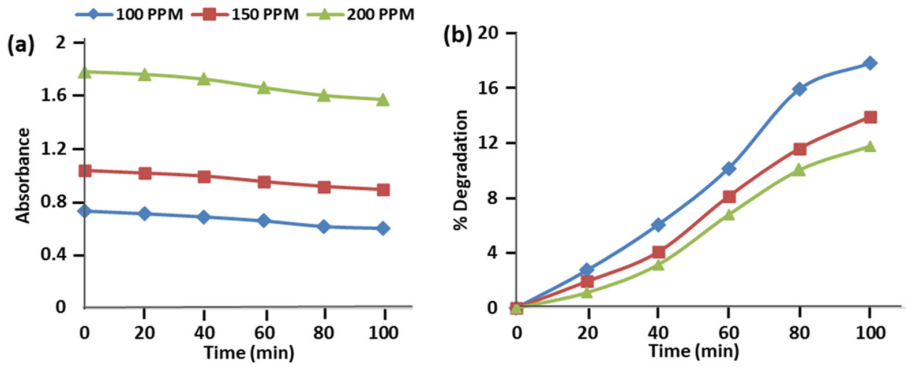

Figure 5. (**a**) Measured absorbance and (**b**) degradation percentage of RO16 solution versus time for various concentrations of the dye without the photocatalyst and under UV irradiation only.

2.2.2. Effect of H_2O_2 Addition on the Degradation of RO16 under UV Irradiation

Further, the effect of adding 0.5 mL H_2O_2 on the decolorization rate of RO16 was investigated. The decomposition percentage of RO16 was slightly enhanced when H_2O_2 was present in the dye solution, reaching 22.5% after 100 min for the 200 ppm dye, as shown in Figure 6b. The enhancement was observed for all dye concentrations. It has been reported that H_2O_2 is able to absorb UV light and generate •OH via its photolysis [40].

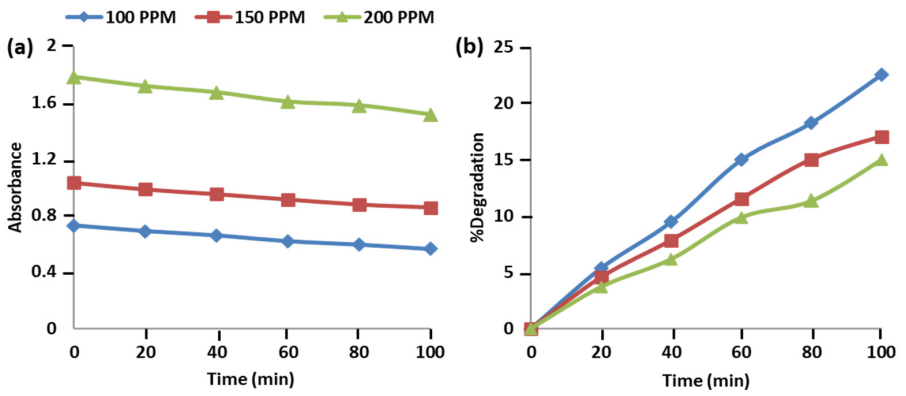

Figure 6. (**a**) Measured absorbance and (**b**) degradation percentages of RO16 solution over time for various concentrations of the dye in the presence of H_2O_2 under UV irradiation without a catalyst.

The development of more $^{\bullet}OH$ would promote the attack on the aromatic ring of RO16 and increase its decomposition rate. Moreover, species of $HO_2^{\bullet}$ can be generated from the scavenging of $^{\bullet}OH$ radicals by H_2O_2. In the presence of H_2O_2 and UV light, the following chain reactions occur, generating highly reactive radicals [41]:

Initiation:

$$H_2O_2 + OH^{\bullet} \rightarrow H_2O + HO_2^{\bullet} \quad (3)$$

Propagation:

$$H_2O + HO_2^{\bullet} \rightarrow H_2O_2 \quad (4)$$

Termination:

$$OH^{\bullet} + OH^{\bullet} \rightarrow H_2O_2 \quad (5)$$

$$HO_2^{\bullet} + HO_2^{\bullet} \rightarrow O_2 + H_2O_2 \quad (6)$$

$$OH^{\bullet} + HO_2^{\bullet} \rightarrow H_2O + O_2 \quad (7)$$

2.2.3. Evaluating the Photocatalytic Activity of ZnO, Bi_2O_3, and ZnO-Bi_2O_3

To explore whether a synergistic effect in the synthesized ZnO-Bi_2O_3 heterojunction prevails, the photocatalytic activity of ZnO-Bi_2O_3 to RO16 dye was compared with individual ZnO and Bi_2O_3 samples, as shown in Figure 7a. Notably, under UV irradiation, Bi_2O_3 alone showed a small degradation efficiency (10%) after 100 min, whilst ZnO exhibited relatively larger degradation efficiency (27%). This observation aligns with the pH-dependent photocatalytic activity of Bi_2O_3. The limited discoloration effect of Bi_2O_3 is most likely because Bi_2O_3 exhibits the optimal decolorization performance in acidic solutions and not at neutral pH values, aligning with previous studies [42]. On the other hand, the ZnO-Bi_2O_3 composite outperformed both Bi_2O_3 and ZnO with degradation % of 29%, indicating a synergistic effect between the two components in their mixture. This result agrees with previous reports [20]. Furthermore, the degradation kinetics were studied by plotting $ln(C_o/C)$ against time (t) for the three different photocatalysts. As displayed in Figure 7b, the data analysis of all samples revealed a linear dependence with correlation coefficients R^2 of 0.997, 0.994, and 0.968, respectively. This adequate linearity demonstrates first-order reaction kinetics for the degradation of the dye RO16, according to the following equation:

$$ln\left(\frac{C_0}{C}\right) = kt \quad (8)$$

where C_0 represents the initial concentration of RO16, C is the concentration at time t, and k is the reaction rate constant. The obtained rate constants were 0.001, 0.003, and 0.004 min^{-1} for Bi_2O_3, ZnO, and ZnO-Bi_2O_3, respectively, as depicted in Figure 7b. This result demonstrates that the ZnO-Bi_2O_3 heterojunction was 300% and 33% faster than Bi_2O_3 and ZnO, respectively; an effect that is indicative of a synergistic interaction between ZnO and Bi_2O_3. These results suggest the ZnO-Bi_2O_3 composite's potential for efficient dye degradation, and therefore, the composite was further investigated in this study.

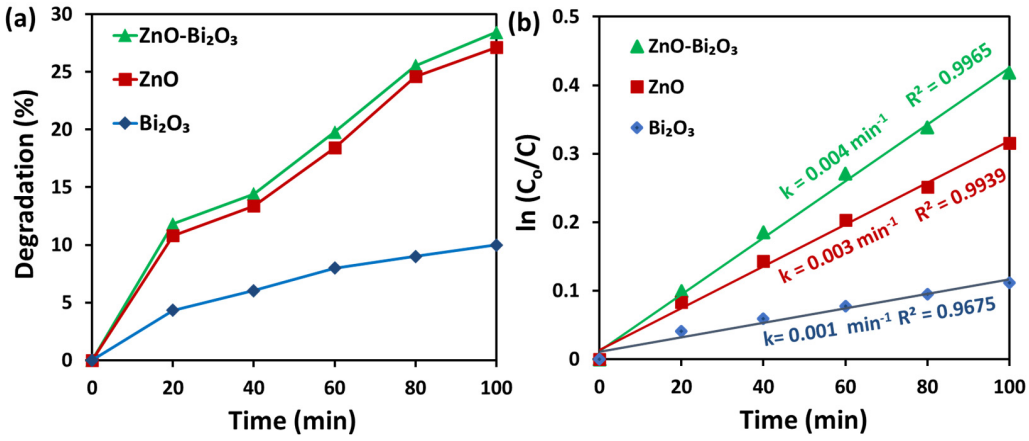

Figure 7. Comparison of (**a**) the degradation efficiency and (**b**) the degradation kinetics of ZnO, Bi_2O_3, and ZnO-Bi_2O_3 catalysts for 100 ppm RO16 solution under UV irradiation.

2.2.4. Effect of RO16 Dye Concentration on the Activity of the ZnO-Bi_2O_3 Photocatalyst under UV Irradiation

To study this effect, aqueous solutions of RO16 dye with various concentrations were irradiated with UV light for different durations in the presence of 0.2 g of the ZnO-Bi_2O_3 catalyst. Figure 8 shows the recorded absorbance and the respective decolorization percentages. In the presence of ZnO-Bi_2O_3, the dye degradation was increased to 28.4% compared to 18% without a catalyst after 100 min of illumination (Figure 8b). This confirms the effectiveness of this photocatalyst in the decolorization of RO16. It is well established that the photocatalytic processes utilizing UV irradiated semiconductors offer a promising approach for the degradation of various organic compounds rather than just photolysis, resulting in the formation of CO_2, H_2O, and associated mineral acids [43]. As discussed below in Figure 9, when photons from UV light with energy equal to or greater than the band gap energy of the semiconductor strike the semiconductor particles, electrons in the conduction band and holes in the valence band are generated. These holes can oxidize water to $OH^{\bullet}$, while the electrons can be consumed by reducible species, such as O_2, in the solution, generating $O_2^{-\bullet}$ [28]. The $^{\bullet}OH$, a highly reactive oxidizing reagent, is commonly responsible for the decomposition of most organic pollutants. In the case of heterostructures like ZnO-Bi_2O_3, the improved photocatalytic performance could be attributed to the extension of the absorption range to the visible light and the reduced recombination rate of the photoinduced electron–hole pairs in the semiconductor Bi_2O_3 with the introduction of ZnO into the heterostructure [44,45].

2.2.5. Effect of H_2O_2 on the Degradation Rate under UV Irradiation at ZnO-Bi_2O_3

To investigate whether a synergistic effect between UV irradiation and H_2O_2 in the presence of ZnO-Bi_2O_3 could boost the decolorization percentage, the absorbance was measured for this system, as displayed in Figure 9a. Figure 9b shows an increased degradation to 48.5% after 200 min, which is significantly higher compared to the individual components. Although the absolute degradation efficiency values did not reach 100% in the studied time, the focus of this study was to understand the synergistic effect created by combining ZnO with Bi_2O_3 and exploring the role of the H_2O_2 oxidant in the improvement of the photodegradation performance. This synergistic effect was attributed to an increased surface area, facilitating effective reactant absorption and enhanced electron–hole generation due to UV light absorption. The combination of these factors led to a more efficient degradation of the dye, highlighting the promising potential of this approach for effective pollutant removal in wastewater treatment applications.

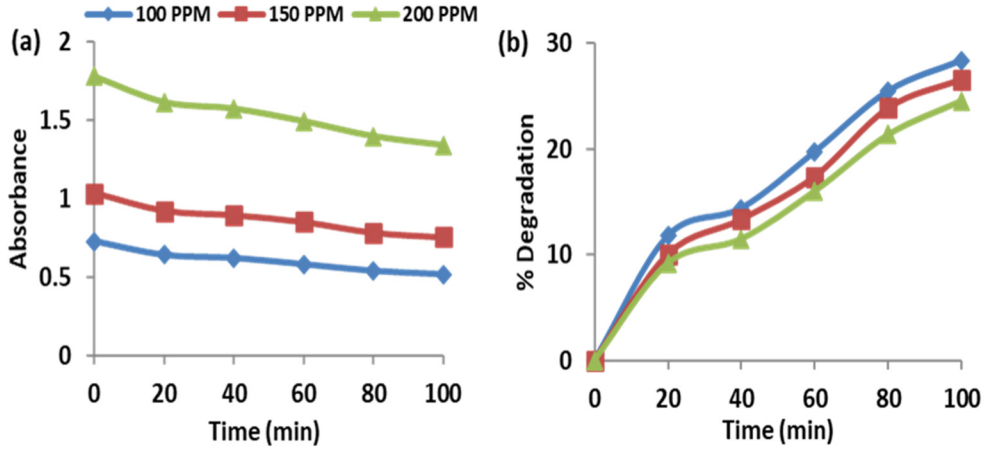

Figure 8. (**a**) Measured absorbance and (**b**) degradation percentage of the RO16 solution over time for various concentrations of the dye in the presence of the ZnO-Bi_2O_3 catalyst under UV irradiation.

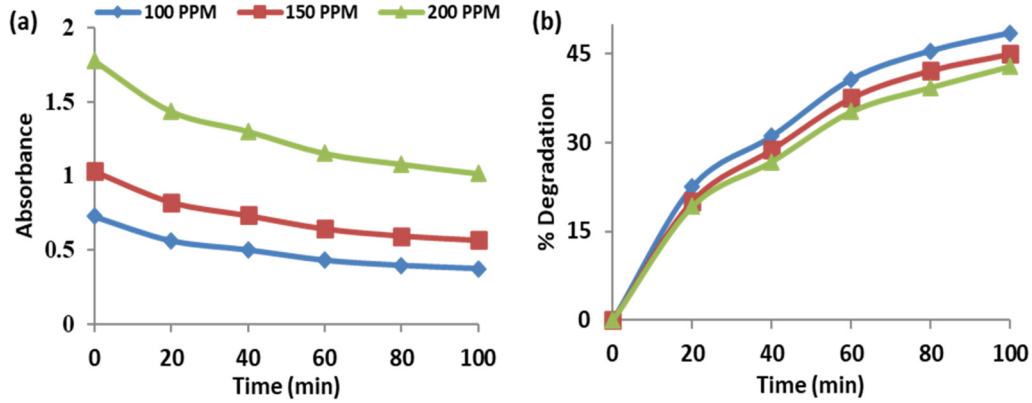

Figure 9. (**a**) Measured absorbance and (**b**) degradation percentage of the RO16 solution over time for various concentrations of the dye in the presence of H_2O_2 and the ZnO-Bi_2O_3 catalyst.

2.2.6. Comparison of the Degradation Performance and Kinetics for RO16 under Different Reaction Conditions

Figure 10a compares the degradation percentage for a 100 ppm aqueous solution of RO16 dye under the different studied conditions. The UV light irradiation alone without H_2O_2 or the photocatalyst resulted in a degradation of only 17.8% after 100 min, indicating minimal photo-induced self-sensitized photolysis of RO16. On the other hand, the addition of the oxidant H_2O_2 to the dye solution improved the degradation percentage from 17.8% to 22.5%, still in the absence of the photocatalyst. The addition of the ZnO-Bi_2O_3 catalyst to the dye solution during UV irradiation without H_2O_2 further boosted the degradation to 28.4%. Interestingly, the most significant enhancement occurred when both the ZnO-Bi_2O_3 photocatalyst and H_2O_2 were present, achieving 48.5% degradation. The enhancement effect of H_2O_2 was much more obvious in the presence of the photocatalyst than in its absence. This could be attributed to the larger surface area of the catalyst available for more H_2O_2 and UV adsorption and thus for more generated active radicals and, accordingly, more degradation. These findings demonstrate the role of the synergistic effect between UV irradiation, the ZnO-Bi_2O_3 catalyst, and H_2O_2 in enhancing RO16 dye decolorization, rendering this approach promising in wastewater treatment and pollution remediation.

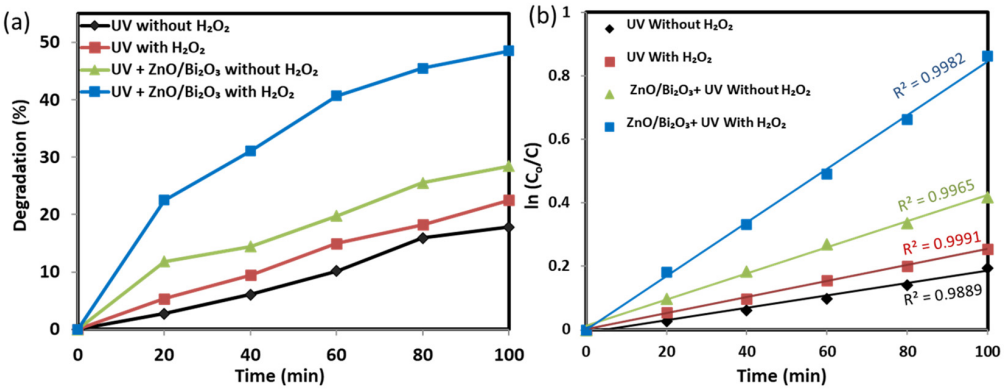

Figure 10. Comparison of the degradation efficiency (**a**) and the corresponding degradation kinetics (**b**) for RO16 dye using UV irradiation alone or UV + ZnO-Bi_2O_3 catalyst with and without the addition of H_2O_2.

Further, the rate constants of RO16 degradation for the different studied cases were determined, as depicted in Figure 10b. The fitting of the data revealed a straight line with correlation coefficients R^2 in the range of 0.989 to 0.999, evidencing first-order reaction kinetics, according to Equation 8. As presented in Table 1, the obtained rate constants (k) varied with experimental conditions as follows: the highest for the combined UV radiation+ ZnO-Bi_2O_3 catalyst + H_2O_2 (0.008 min^{-1}); followed by UV radiation + ZnO-Bi_2O_3 catalyst without H_2O_2 (0.004 min^{-1}); then UV radiation with H_2O_2 (0.003 min^{-1}); and the lowest for UV radiation alone (0.002 min^{-1}). The results show that the addition of H_2O_2 doubled the degradation rate under UV irradiation. The presence of the ZnO-Bi_2O_3 photocatalyst led to at least a two-fold higher degradation efficiency than its absence, indicating the effect of the photocatalyst on the process. Hence, by combining UV, ZnO-Bi_2O_3, and H_2O_2, the highest performance was achieved due to a possible synergistic effect between the individual factors.

Table 1. Rate constant values for the degradation of RO16 dye using UV radiation, H_2O_2, and the photocatalyst ZnO-Bi_2O_3 under different conditions.

	UV without H_2O_2	**UV with H_2O_2**	**ZnO-Bi_2O_3 +UV without H_2O_2**	**ZnO-Bi_2O_3 + UV with H_2O_2**
***k* (min^{-1})**	0.002	0.003	0.004	0.008
R^2	0.989	0.999	0.997	0.998

2.2.7. Proposed Mechanism of Photocatalytic Activity at ZnO-Bi_2O_3

In photocatalytic applications, the interface between ZnO and Bi_2O_3 plays a pivotal role in facilitating charge transfer processes and electron–hole pair separation when exposed to UV light as well as the H_2O_2 oxidant. A general proposed mechanism of the photocatalysis at ZnO-Bi_2O_3 is presented in Figure 11. The given energy values of band gaps of individual materials as well as the valence band (VB) and the conduction band (CB) in Figure 11 were sourced from the literature [15,20,46,47]. When the photocatalyst is UV-irradiated, electron–hole pairs are created in the system. Importantly, the relative energy levels at the interface of this system enable the efficient transfer of electrons from the CB of Bi_2O_3 to that of ZnO, while holes migrate from the VB of ZnO to Bi_2O_3, as shown in Figure 11. This charge transfer phenomenon predominantly occurs in the vicinity of Bi_2O_3, thus effectively mitigating recombination events and optimizing charge separation [20]. The redox potentials of expected reactions in (V) and their corresponding values on the absolute voltage scale (AVS) in (eV) are also displayed in Figure 11. Upon UV light illumination, both ZnO and Bi_2O_3 generate electron–hole pairs. The ZnO-Bi_2O_3 interface acts as a platform for the spatial separation of these photogenerated carriers. Subsequently,

the separated electrons and holes are harnessed to initiate reactions with adsorbed oxygen species on the photocatalyst surface, yielding reactive oxygen species (ROS). Namely, the potential energy of holes in the valence band (3.07 V) of ZnO is sufficiently positive to drive the oxidation of water, producing hydroxyl radicals ($^{\bullet}OH$) as follows [46]:

$$H_2O + h^+ \rightarrow {}^{\bullet}OH + H^+ \qquad E^o = 2.31\ V \tag{9}$$

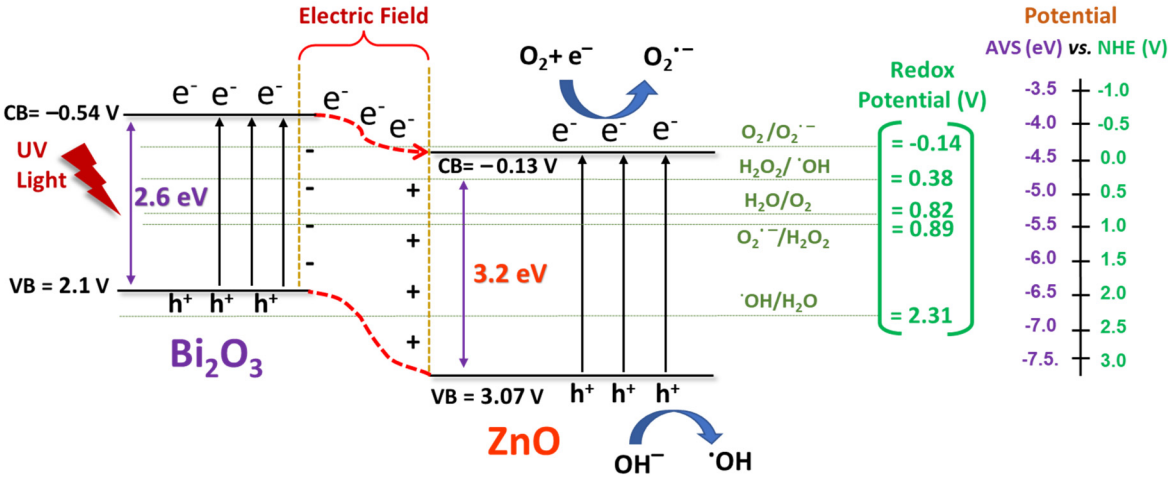

Figure 11. Schematic drawing of the proposed band structure diagram depicting the energy levels of ZnO and Bi_2O_3, along with the expected reactions when ZnO-Bi_2O_3 is exposed to UV light.

Furthermore, electrons residing in the conduction band of ZnO or Bi_2O_3 can oxidize dissolved oxygen, generating superoxide radicals ($O_2^{\bullet-}$) as follows [46,48]:

$$O_2 + e^- \rightarrow O_2^{\bullet-} \qquad E^o = -0.14\ V \tag{10}$$

The redox potential of this oxidation process (−0.14 V) matches the energy of the CB of Bi_2O_3 (−0.13 V). The produced superoxide may directly contribute to degradation processes of the dye or further promote hydroxyl radical formation [20]. Moreover, the addition of H_2O_2 as an oxidizing agent to the reaction solution could also contribute to the production of $^{\bullet}OH$ and $O_2^{\bullet-}$ radicals, as discussed above [46]. The produced ROS radicals react with the dye, degrading it. It was reported that $O_2^{\bullet-}$ are the primary radicals for different dye degradation [27]. The synergy of these pathways for $^{\bullet}OH$ and $O_2^{\bullet-}$ production would contribute to a swift degradation reaction rate and high levels of degradation, highlighting the potential of ZnO-Bi_2O_3 heterojunctions in advanced photocatalytic applications.

3. Materials and Methods

3.1. Chemicals

Potassium dichromate ($K_2Cr_2O_7$), acetic acid, zinc chloride ($ZnCl_2$), bismuth nitrate pentahydrate ($Bi(NO_3)_3{\cdot}5H_2O$), sodium hydroxide, and hydrogen peroxide were of analytical grade. RO16 dye was purchased from Sigma-Aldrich (St. Louis, MO, USA). All chemicals were used without further purification. All solutions were prepared in distilled water.

3.2. Synthesis of ZnO-Bi_2O_3 Particles

To synthesize the ZnO-Bi_2O_3 composite catalyst with 10 mol% Bi_2O_3, a simple previously reported chemical co-precipitation method was conducted with slight modification [49]. First, 0.09 M $ZnCl_2$ and 0.01 M ($Bi(NO_3)_3{\cdot}5H_2O$) solutions were prepared. Both solutions were mixed and heated under constant stirring to attain 80 °C. Then, 2 mL of acetic acid was added to the heated solution and subsequently, 1M NaOH was added drop-

wise with vigorous stirring until pH 7 was obtained and precipitation started to occur. The solution was further stirred at 80 °C for one hour. Afterward, the solution was cooled down and the precipitate was collected, washed, and dried. Finally, the precipitate was calcined in a furnace at 400 °C for 2 h, yielding ZnO-Bi_2O_3 microparticles. This procedure has been reported to yield about 9:1 weight ratio of ZnO:Bi_2O_3 in the formed heterostructure [49].

3.3. Characterization of ZnO-Bi_2O_3 Particles

Fourier transform infrared (FTIR) spectra of the as-prepared photo-catalyst were determined using a FTIR spectrophotometer (Bruker Tensor 27) in the range of 400–4000 cm^{-1}. Powder X-ray diffraction (XRD) analysis was carried out to determine the crystallinity and crystalline structure of the synthesized material. XRD patterns of the synthesized powder were recorded on a Rigaku D/Max-IIIA diffractometer (Rigaku Co., Tokyo, Japan) with copper Kα radiation of a wavelength of 1.54051 Å. To study the morphology of the samples, scanning electron microscope (SEM) analysis was carried out using an JEOL LEO 44i instrument, which was operated at 10 kV. EDX analysis was conducted on a Nova NanoSEM 450 equipped with EDX instrument operating at 25 kV. For UV–Vis analysis, a twin beam spectrophotometer (Rayleigh-UV2601) was used.

3.4. Photocatalytic Degradation Measurements

Initially, the maximum absorbance wavelength (λ_{max}) of the RO16 dye was determined by recording UV–Vis spectra for 100 ppm solution. The samples were scanned in the range of 200–800 nm. The photolytic and photocatalytic activity of RO16 in aqueous solution under UV light were investigated. The photolytic measurements were conducted via the irradiation of the RO16 solution using a UV lamp with 144 watt intensity and a wavelength of 244 nm. The UV absorbance values of a portion of the solution were recorded until 100 min with a time interval of 20 min. Three concentrations of the dye aqueous solution were studied.

For the photocatalytic activity measurements, the ZnO-Bi_2O_3 catalyst (0.2 g) was added to the dye solution and the solution was investigated under the same conditions for comparison. All experiments were performed in Pyrex glass batch reactors (50 mL solution) under constant magnetic stirring. After irradiation with UV light, 0.5 mL of the dye solution was withdrawn at 0 (before irradiation), 20, 40, 60, 80 and 100 min and their absorbance at a wavelength of 490 nm were measured using a UV–Vis spectrophotometer. In addition, the effect of hydrogen peroxide on the degradation rate of RO16 was studied, where 0.5 mL H_2O_2 was added to the dye solution and the absorbance was measured under the same conditions. The degradation efficiency in % of the dye was calculated using the following equation.

$$\%\ Degradation = \frac{A_0 - A}{A_0} \times 100 = \frac{C_0 - C}{C_0} \times 100 \quad (11)$$

where A_0 and A are the absorbance of the dye solution before and after the UV irradiation of the dye solution for time t, respectively. C_0 and C represent the respective concentrations of the dye before and after the irradiation of the dye solution, respectively.

4. Conclusions

The textile industry releases hazardous chemicals, including carcinogenic reactive dyes, contributing to water pollution. Conventional degradation methods such as chemical oxidation and biodegradation have limitations in addressing this issue effectively. Photocatalysis using semiconductors provides an efficient alternative. In this study, ZnO-Bi_2O_3 composite clusters were successfully synthesized using a facile co-precipitation method and were then investigated as photocatalysts for the photocatalytic degradation of reactive Orange 16 (RO16) dye, a model textile azo dye. The presence of the ZnO-Bi_2O_3 photocatalyst in the solution doubled the decolorization rate of RO16 compared to UV irradiation alone. The degradation rate via the ZnO-Bi_2O_3 heterojunction was more efficient and around 300

and 33% faster than individual Bi_2O_3 and ZnO catalysts, respectively. Furthermore, the addition of the oxidant H_2O_2 with UV irradiation amplified the degradation rate up to two times compared to only UV light, leading to a significant improvement in the oxidation and remediation of RO16. The positive effect of H_2O_2 could be ascribed to the generation of more oxygen radicals that effectively decomposed the dye, where H_2O_2 could be decomposed to $^{\bullet}OH$ or react with produced $^{\bullet}OH$, forming $HO_2^{\bullet}$ radicals. The degradation process followed first-order reaction kinetics with a rate constant of 0.008 min^{-1} in the case of ZnO-Bi_2O_3 + UV + H_2O_2. Hence, the present study reveals the impact of combining UV radiation, H_2O_2, and the ZnO-Bi_2O_3 catalyst to achieve a synergistic effect and improved photocatalytic performance. This innovative approach holds promise for combating water pollution caused by textile industry dyes.

Author Contributions: R.S.: investigation, methodology, formal analysis; M.M.: supervision, conceptualization, resources, review and editing; R.K.: writing—original draft, visualization, review and editing; H.M.A.A.: data interpretation; visualization, writing—review and editing. All authors have read and agreed to the published version of the manuscript.

Funding: The authors acknowldege the support from Government College University Faisalabad (Pakistan) and Cairo University (Egypt).

Data Availability Statement: Data are available upon reasonable request from the authors.

Conflicts of Interest: The authors declare no conflict of interest.

References

1. Bhatia, S.; Devraj, S. *Pollution Control in Textile Industry*; WPI Publishing: New Delhi, India, 2017.
2. Gita, S.; Hussan, A.; Choudhury, T. Impact of textile dyes waste on aquatic environments and its treatment. *Environ. Ecol.* **2017**, *35*, 2349–2353.
3. Kant, R. Textile dyeing industry an environmental hazard. *Nat. Sci.* **2012**, *4*, 22–26. [CrossRef]
4. Amin, H.M.; El-Kady, M.F.; Atta, N.F.; Galal, A. Gold nanoparticles decorated graphene as a high performance sensor for determination of trace hydrazine levels in water. *Electroanalysis* **2018**, *30*, 1757–1766. [CrossRef]
5. Hassan, M.M.; Carr, C.M. A critical review on recent advancements of the removal of reactive dyes from dyehouse effluent by ion-exchange adsorbents. *Chemosphere* **2018**, *209*, 201–219. [CrossRef]
6. Slokar, Y.M.; Le Marechal, A.M. Methods of decoloration of textile wastewaters. *Dyes Pigm.* **1998**, *37*, 335–356. [CrossRef]
7. Santoso, E.; Ediati, R.; Kusumawati, Y.; Bahruji, H.; Sulistiono, D.; Prasetyoko, D. Review on recent advances of carbon based adsorbent for methylene blue removal from waste water. *Mater. Today Chem.* **2020**, *16*, 100233. [CrossRef]
8. Brüninghoff, R.; Van Duijne, A.K.; Braakhuis, L.; Saha, P.; Jeremiasse, A.W.; Mei, B.; Mul, G. Comparative analysis of photocatalytic and electrochemical degradation of 4-ethylphenol in saline conditions. *Environ. Sci. Technol.* **2019**, *53*, 8725–8735. [CrossRef]
9. Premaratne, M.; Nishshanka, G.; Liyanaarachchi, V.; Nimarshana, P.; Ariyadasa, T.U. Bioremediation of textile dye wastewater using microalgae: Current trends and future perspectives. *J. Chem. Technol. Biotechnol.* **2021**, *96*, 3249–3258. [CrossRef]
10. Dihom, H.R.; Al-Shaibani, M.M.; Mohamed, R.M.S.R.; Al-Gheethi, A.A.; Sharma, A.; Khamidun, M.H.B. Photocatalytic degradation of disperse azo dyes in textile wastewater using green zinc oxide nanoparticles synthesized in plant extract: A critical review. *J. Water Process. Eng.* **2022**, *47*, 102705. [CrossRef]
11. Wang, J.; Li, R.; Zhang, Z.; Sun, W.; Xu, R.; Xie, Y.; Xing, Z.; Zhang, X. Efficient photocatalytic degradation of organic dyes over titanium dioxide coating upconversion luminescence agent under visible and sunlight irradiation. *Appl. Catal. A Gen.* **2008**, *334*, 227–233. [CrossRef]
12. Atta, N.F.; Galal, A.; Amin, H.M. Synthesis and photoelectrochemical behavior of a hybrid electrode composed of polyaniline encapsulated in highly ordered TiO_2 nanotubes array. *Int. J. Electrochem. Sci.* **2012**, *7*, 3610–3626.
13. Atta, N.F.; Amin, H.M.; Khalil, M.W.; Galal, A. Nanotube arrays as photoanodes for dye sensitized solar cells using metal phthalocyanine dyes. *Int. J. Electrochem. Sci.* **2011**, *6*, 3. [CrossRef]
14. Li, X.; Wang, D.T.; Chen, J.F.; Tao, X. Enhanced photosensitized degradation of organic pollutants under visible radiation by (I2) n-encapsulated TiO2 films. *Ind. Eng. Chem. Res.* **2012**, *51*, 1110–1117. [CrossRef]
15. Ghaffar, S.; Abbas, A.; Naeem-ul-Hassan, M.; Assad, N.; Sher, M.; Ullah, S.; Alhazmi, H.A.; Najmi, A.; Zoghebi, K.; Al Bratty, M.; et al. Improved Photocatalytic and Antioxidant Activity of Olive Fruit Extract-Mediated ZnO Nanoparticles. *Antioxidants* **2023**, *12*, 1201. [CrossRef]
16. Al-Zahrani, S.A.; Patil, M.B.; Mathad, S.N.; Patil, A.Y.; Otaibi, A.A.; Masood, N.; Mansour, D.; Khan, A.; Manikandan, A.; Syafri, E. Photocatalytic Degradation of Textile Orange 16 Reactive Dye by ZnO Nanoparticles Synthesized via Green Route Using Punica Granatum Leaf Extract. *Crystals* **2023**, *13*, 172. [CrossRef]

17. Wang, P.; Wang, S.-Z.; Kang, Y.-R.; Sun, Z.-S.; Wang, X.-D.; Meng, Y.; Hong, M.-H.; Xie, W.-F. Cauliflower-shaped Bi2O3–ZnO heterojunction with superior sensing performance towards ethanol. *J. Alloys Compd.* **2021**, *854*, 157152. [CrossRef]
18. Toledo Arana, J.; Torres, J.J.; Acevedo, D.F.; Illanes, C.O.; Ochoa, N.A.; Pagliero, C.L. One-step synthesis of CaO-ZnO efficient catalyst for biodiesel production. *Int. J. Chem. Eng.* **2019**, *2019*, 1806017. [CrossRef]
19. Balachandran, S.; Swaminathan, M. Facile fabrication of heterostructured Bi_2O_3–ZnO photocatalyst and its enhanced photocatalytic activity. *J. Phys. Chem. C* **2012**, *116*, 26306–26312. [CrossRef]
20. Medina, J.; Portillo-Vélez, N.; Bizarro, M.; Hernández-Gordillo, A.; Rodil, S. Synergistic effect of supported ZnO/Bi_2O_3 heterojunctions for photocatalysis under visible light. *Dyes Pigm.* **2018**, *153*, 106–116. [CrossRef]
21. Wen, L.; Wang, D.; Xi, J.; Tian, F.; Liu, P.; Bai, Z.-W. Heterometal modified Fe_3O_4 hollow nanospheres as efficient catalysts for organic transformations. *J. Catal.* **2022**, *413*, 779–785. [CrossRef]
22. Wang, D.; Li, Y.; Wen, L.; Xi, J.; Liu, P.; Hansen, T.W.; Li, P. Ni-Pd-incorporated Fe_3O_4 yolk-shelled nanospheres as efficient magnetically recyclable catalysts for reduction of n-containing unsaturated compounds. *Catalysts* **2023**, *13*, 190. [CrossRef]
23. Li, L.; Zhang, L.; Gou, L.; Wei, S.; Hou, X.; Wu, L. Au Nanoparticles Decorated CoP Nanowire Array: A Highly Sensitive, Anticorrosive, and Recyclable Surface-Enhanced Raman Scattering Substrate. *Anal. Chem.* **2023**, *95*, 11037–11046. [CrossRef] [PubMed]
24. Mottola, S.; Mancuso, A.; Sacco, O.; Vaiano, V.; De Marco, I. Photocatalytic Systems Based on ZnO Produced by Supercritical Antisolvent for Ceftriaxone Degradation. *Catalysts* **2023**, *13*, 1173. [CrossRef]
25. Boudalia, M.; Laourayed, M.; El Moudane, M.; Sekkat, Z.; Campos, O.S.; Bellaouchou, A.; Guenbour, A.; Garcia, A.J.; Amin, H.M. Phosphate glass doped with niobium and bismuth oxides as an eco-friendly corrosion protection matrix of iron steel in HCl medium: Experimental and theoretical insights. *J. Alloys Compd.* **2023**, *938*, 168570. [CrossRef]
26. Jiang, H.Y.; Liu, J.; Cheng, K.; Sun, W.; Lin, J. Enhanced visible light photocatalysis of Bi_2O_3 upon fluorination. *J. Phys. Chem. C* **2013**, *117*, 20029–20036. [CrossRef]
27. Wang, X.; Ren, P.; Fan, H. Room-temperature solid state synthesis of ZnO/Bi_2O_3 heterojunction and their solar light photocatalytic performance. *Mater. Res. Bull.* **2015**, *64*, 82–87. [CrossRef]
28. Amin, H.M.; Molls, C.; Bawol, P.P.; Baltruschat, H. The impact of solvent properties on the performance of oxygen reduction and evolution in mixed tetraglyme-dimethyl sulfoxide electrolytes for Li-O_2 batteries: Mechanism and stability. *Electrochim. Acta* **2017**, *245*, 967–980. [CrossRef]
29. Ramachandran, S.; Sivasamy, A. Effective charge separation in binary ZnO-Bi_2O_3 photocatalytic material for the treatment of simulated wastewater. *Mater. Today Proc.* **2019**, *17*, 101–110. [CrossRef]
30. Georgiou, D.; Melidis, P.; Aivasidis, A.; Gimouhopoulos, K. Degradation of azo-reactive dyes by ultraviolet radiation in the presence of hydrogen peroxide. *Dyes Pigm.* **2002**, *52*, 69–78. [CrossRef]
31. Ali, A.; Biswas, M.R.U.D.; Oh, W.C. Novel and simple process for the photocatalytic reduction of CO_2 with ternary Bi_2O_3–graphene–ZnO nanocomposite. *J. Mater. Sci. Mater. Electron.* **2018**, *29*, 10222–10233. [CrossRef]
32. Reddy, K.H.; Martha, S.; Parida, K. Facile fabrication of Bi_2O_3/Bi–$NaTaO_3$ photocatalysts for hydrogen generation under visible light irradiation. *RSC Adv.* **2012**, *2*, 9423–9436. [CrossRef]
33. Premalatha, N.; Miranda, L.R. Surfactant modified ZnO–Bi_2O_3 nanocomposite for degradation of lambda-cyhalothrin pesticide in visible light: A study of reaction kinetics and intermediates. *J. Environ. Manag.* **2019**, *246*, 259–266. [CrossRef] [PubMed]
34. Shandilya, P.; Sudhaik, A.; Raizada, P.; Hosseini-Bandegharaei, A.; Singh, P.; Rahmani-Sani, A.; Thakur, V.; Saini, A.K. Synthesis of eu3+− doped zno/bi2o3 heterojunction photocatalyst on graphene oxide sheets for visible light-assisted degradation of 2, 4-dimethyl phenol and bacteria killing. *Solid State Sci.* **2020**, *102*, 106164. [CrossRef]
35. Saritha, D.; Markandeya, Y.; Salagram, M.; Vithal, M.; Singh, A.; Bhikshamaiah, G. Effect of Bi_2O_3 on physical, optical and structural studies of ZnO–Bi_2O_3–B_2O_3 glasses. *J. Non Cryst. Solids* **2008**, *354*, 5573–5579. [CrossRef]
36. Ullah, S.; Khalid, R.; Rehman, M.F.; Irfan, M.I.; Abbas, A.; Alhoshani, A.; Anwar, F.; Amin, H. Biosynthesis of phyto-functionalized silver nanoparticles using olive fruit extract and evaluation of their antibacterial and antioxidant properties. *Front. Chem.* **2023**, *11*, 1202252. [CrossRef]
37. Dhahri, I.; Ellouze, M.; Labidi, S.; Al-Bataineh, Q.M.; Etzkorn, J.; Guermazi, H.; Telfah, A.; Tavares, C.J.; Hergenröder, R.; Appel, T. Optical and structural properties of ZnO NPs and ZnO–Bi_2O_3 nanocomposites. *Ceram. Int.* **2022**, *48*, 266–277. [CrossRef]
38. Pankove, J.I. *Optical Processes in Semiconductors*; Courier Corporation: Mineola, NY, USA, 1975.
39. Jamal, M.A.; Muneer, M.; Iqbal, M. Photo-degradation of monoazo dye blue 13 using advanced oxidation process. *Chem. Int* **2015**, *1*, 12–16.
40. Mitrović, J.Z.; Radović, M.D.; Anđelković, T.D.; Bojić, D.V.; Bojić, A.L. Identification of intermediates and ecotoxicity assessment during the UV/H_2O_2 oxidation of azo dye Reactive Orange 16. *J. Environ. Sci. Health A* **2014**, *49*, 491–502. [CrossRef]
41. Bokhari, T.H.; Kashif, M.; Bhatti, I.A.; Zubair, M.; Adeel, S.; Yousaf, M.; Ahmad, M.; Iqbal, M.; Usman, M.; Zuber, M. Degradation Study of CI Reactive Yellow 145 by Advanced Oxidation Process. *Asian J. Chem.* **2013**, *25*, 8668–8672. [CrossRef]
42. Medina, J.; Bizarro, M.; Gomez, C.; Depablos-Rivera, O.; Mirabal-Rojas, R.; Monroy, B.; Fonseca-Garcia, A.; Perez-Alvarez, J.; Rodil, S. Sputtered bismuth oxide thin films as a potential photocatalytic material. *Catal. Today* **2016**, *266*, 144–152. [CrossRef]
43. Trandafilović, L.V.; Jovanović, D.J.; Zhang, X.; Ptasińska, S.; Dramićanin, M. Enhanced photocatalytic degradation of methylene blue and methyl orange by ZnO: Eu nanoparticles. *Appl. Catal. B Environ.* **2017**, *203*, 740–752. [CrossRef]

44. Liu, X.; Pan, L.; Lv, T.; Sun, Z.; Sun, C.Q. Visible light photocatalytic degradation of dyes by bismuth oxide-reduced graphene oxide composites prepared via microwave-assisted method. *J. Colloid Interface Sci.* **2013**, *408*, 145–150. [CrossRef] [PubMed]
45. Landge, V.; Sonawane, S.; Sivakumar, M.; Sonawane, S.; Babu, G.U.B.; Boczkaj, G. S-scheme heterojunction Bi_2O_3-ZnO/Bentonite clay composite with enhanced photocatalytic performance. *Sustain. Energy Technol. Assess* **2021**, *45*, 101194. [CrossRef]
46. Foote, C.S.; Valentine, J.S.; Greenberg, A.; Liebman, J.F. *Active Oxygen in Chemistry*; Springer Science & Business Media: Berlin/Heidelberg, Germany, 2012; Volume 2.
47. Guo, J.-G.; Liu, Y.; Hao, Y.-J.; Li, Y.-L.; Wang, X.-J.; Liu, R.-H.; Li, F.-T. Comparison of importance between separation efficiency and valence band position: The case of heterostructured Bi_3O_4Br/α-Bi_2O_3 photocatalysts. *Appl. Catal. B Environ.* **2018**, *224*, 841–853. [CrossRef]
48. Liu, C.; Mao, S.; Wang, H.; Wu, Y.; Wang, F.; Xia, M.; Chen, Q. Peroxymonosulfate-assisted for facilitating photocatalytic degradation performance of 2D/2D WO_3/BiOBr S-scheme heterojunction. *J. Chem. Eng.* **2022**, *430*, 132806. [CrossRef]
49. Jan, T.; Azmat, S.; Wahid, B.; Adil, M.; Alawadhi, H.; Mansoor, Q.; Farooq, Z.; Ilyas, S.; Ahmad, I.; Ismail, M. Chemically synthesized ZnO-Bi_2O_3 (BZO) nanocomposites with tunable optical, photoluminescence and antibacterial characteristics. *Mater. Sci. Semicond. Process.* **2018**, *84*, 71–75. [CrossRef]